BULLETIN OF THE POLISH ACADEMY OF SCIENCES
TECHNICAL SCIENCES, Vol. 73(1), 2025, Article number: e152209
DOI: 10.24425/bpasts.2024.152209

Fixed switching frequency model predictive control and passivity based control for DC-DC converter

Yajing ZHANG[1]*, Yuqing SHEN[1], BaoYing HUANG[2], Jiangchao ZHANG[2], and Haojing CHANG[3]

[1] School of Automation, Beijing Information Science & Technology University, Beijing, China
[2] State Grid Economic and Technological Research Institute Co., Ltd, Beijing, China
[3] State Grid Corporation Gansu, Power Grid Construction Division, Gansu, China

Abstract. The DC-DC converter represents a crucial component in renewable energy sources. The stability and dynamic capability enhancement of the DC/DC converter have emerged as a significant research topic in the current era. Model predictive control (MPC) is particularly prevalent due to its high dynamic response speed, simplicity of the controller design, and capacity for multi-objective optimization. However, the traditional finite control set model predictive control (FCS-MPC) method suffers as a result of variable switching frequency and vast computing. To improve the dynamic performance of the converter, a novel nonlinear control strategy named fixed switching frequency MPC and passivity-based control (PBC), named FSF-PBMPC, are both proposed. They could allow to achieve fixed switching frequency and to enhance the system's dynamic response speed. Firstly, the Euler-Lagrange (EL) model of the boost converter is established. Secondly, the relationship between duty cycle and MPC is established. Ultimately, the output voltage of PBC is incorporated into the cost function of the FCS-MPC. The characteristics of PBC power shaping and damping injection can enhance the system's immunity to interference, improve the system's dynamic response speed, and thus reinforce the system's stability. Then, depending on MATLAB, the simulation results can prove that the proposed strategy has the effect we expected.

Keywords: DC-DC converter; FCS-MPC; passivity-based control.

1. INTRODUCTION

The growing interest in distributed generation technology has been driven by the emergence of energy scarcity and energy security concerns. As the integration of renewable energy sources, such as photovoltaic and wind power generation, connected to distributed power generation systems, increases, the randomness and volatility of the renewable sources, including enhancing dynamic performance, steady state characteristics, and full load range characteristics of the converter [1, 2], also grow. The DC-DC converter plays an important role as an interface for distributed power generation into the grid, as shown in Fig. 1. Figure 1 illustrates the configuration of a classical DC microgrid, comprising a photovoltaic power generation module, battery module, DC and AC loads. The DC bus voltage level serves as the power processing unit for new energy generation in the microgrid through a converter.

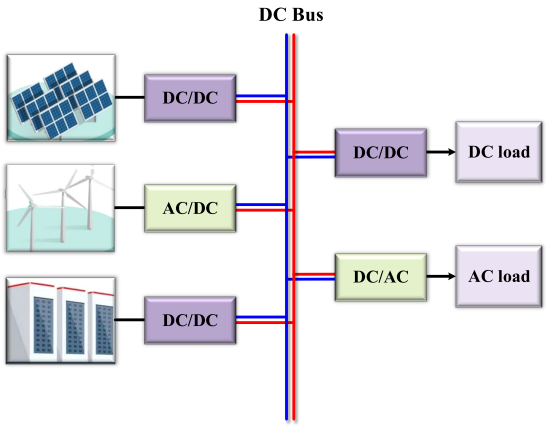

Fig. 1. Schematic diagram of DC microgrid

The nonlinear characteristics of the distributed power generation system, as previously highlighted, present challenges to the traditional linear controllers [3]. The response speed of the control method and the stability of the controlled variables are particularly important for the system. The regulation goal of the DC-DC converter is to reach a stable value of the output voltage. Researchers have proposed a variety of control methods to address the difficulty of regulating the output voltage to a stable value [4, 5]. To better characterize the nonlinear characteristics of systems and improve their dynamic performance, nonlinear control has received widespread attention [6–9]. For example, sliding mode control [10, 11], fuzzy control [12], internal model control [13] and feedback linearization control [14] have all been proposed. Among the aforementioned control strategies, the traditional sliding mode control exhibits high robustness [15]. However, the design of the control signal is more intricate. The utilization of fuzzy control demonstrates improved regulation of the converter with enhanced nonlinear characteristics, as evidenced in the literature [16]. However, the limitation of the fuzzy

*e-mail: zhangyajing@bistu.edu.cn

Manuscript submitted 2024-06-26, revised 2024-09-12, initially accepted for publication 2024-09-25, published in January 2025.

rule design makes the method require re-designing of the rules under varying operating conditions, resulting in an increased number of fuzzy rules and subsequent computational complexity. The literature [17] has devised an IDA-PBC with complementary PI controllers, which eradicates the steady-state error through the implementation of complementary PI controllers. This method offers rapid dynamic response speed, robust immunity to interference and high stability. However, its response speed to external disturbances is relatively slow. In response, literature [18] has proposed a PI-PBC method and utilized a parameter estimation-based observer to estimate the converter inductor current. In recent years, MPC has gained prominence as a predominant control strategy in the electrical field [19], which has advantages in dynamic response speed, immunity and implementation. MPC could be categorized into two distinct groups, including FCS-MPC and continuous control set model predictive control (CCS-MPC) [20,21]. Initially, the FCS-MPC controller had been widely employed in converters because of its simple design, the ability to achieve multi-objective optimization and fast dynamic response [22–25]. However, the traditional FCS-MPC strategy produces variable switching frequency during the control process, which will result in the saturation of boundaries in the inductor circuit ripple, and present a challenge in the design of the filter. Furthermore, fluctuations in the switching frequency may also result in increased energy consumption and a reduction in system efficiency. To tackle this problem, a solution for achieving the fixed switching frequency is raised in [26]. The fixed switching frequency MPC is also employed in literature [27], which achieves control of the fixed switching frequency by adjusting the inductor current ripple variation in the cost function. Nevertheless, the switching frequency continues to fluctuate due to alterations in system parameters.

To address the aforementioned issues, a nonlinear control method that integrates passive theory and fixed switching frequency MPC, named FSF-PBMPC, is proposed in this paper. Firstly, the Euler-Lagrange model of the boost converter is established. Secondly, MPC exports the duty cycle signal. Finally, the PBC output voltage is incorporated into the cost function of the FCS-MPC with fixed switching frequency. The system's dynamic response speed is enhanced by eliminating the necessity for additional control loops, while its immunity to external parameter changes is also improved. This paper uses the boost converter as a model, and the simulation results verify the validity of the method.

This paper is organized as follows. In Section 2, the mathematical model of the boost converter is presented. In Section 3, the model of the FSF-PBMPC is proposed, and it introduces PBC output voltage to the MPC with a fixed switching frequency. In Section 4, the simulation results are analyzed. Finally, the conclusions of this strategy are analyzed in Section 5.

2. MATHEMATICAL MODEL OF THE BOOST CONVERTER

The boost converter can be shown as an example to expand the modeling analysis of the proposed strategy, for the reason that it represents the typical converter. In Fig. 2, the topology of a boost converter is represented, where L is the inductor inductance, C is the capacitor, R represents the load, S represents the main switch, and VD is the diode. Here, i_{in} is the inductor current, u_{in} is the input voltage and u_p is the output voltage.

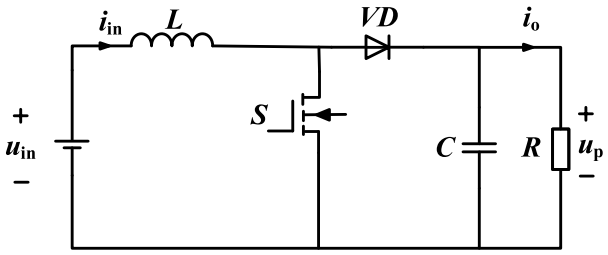

Fig. 2. Boost converter with resistive load

Based on the theory of Kirchhoff, we can get the state-space model of the boost converter in the continuous-time domain which is presented in (1).

$$\begin{cases} L\dfrac{\mathrm{d}i_{\text{in}}}{\mathrm{d}t} = u_{\text{in}} - (1-s)\cdot u_p, \\ C\dfrac{\mathrm{d}u_p}{\mathrm{d}t} = (1-s)\cdot i_{\text{in}} - \dfrac{u_p}{R}. \end{cases} \tag{1}$$

3. IMPLEMENTATION OF THE PROPOSED FSF-PBMPC CONTROLLER

3.1. PBC-based nonlinear design of the boost converter

Before applying the nonlinear control strategy to the central converter, the PBC model of the system should be provided first. Initially, (1) could be expressed as:

$$\boldsymbol{A}\frac{\mathrm{d}\boldsymbol{x}}{\mathrm{d}t} + \boldsymbol{B}\boldsymbol{x} + \boldsymbol{R}\boldsymbol{x} = \boldsymbol{U}, \tag{2}$$

where: $\boldsymbol{A} = \begin{bmatrix} L & 0 \\ 0 & C \end{bmatrix}$, $\boldsymbol{B} = \begin{bmatrix} 0 & 1-s \\ s-1 & 0 \end{bmatrix}$, $\boldsymbol{R} = \begin{bmatrix} 0 & 0 \\ 0 & \dfrac{1}{R} \end{bmatrix}$, $\boldsymbol{U} = \begin{bmatrix} u_{\text{in}} \\ 0 \end{bmatrix}$, $\boldsymbol{x} = \begin{bmatrix} x_1 & x_2 \end{bmatrix}^T = \begin{bmatrix} i_{\text{in}} & u_p \end{bmatrix}^T$, $\dot{\boldsymbol{x}} = \begin{bmatrix} \dfrac{\mathrm{d}x_1}{\mathrm{d}t} & \dfrac{\mathrm{d}x_2}{\mathrm{d}t} \end{bmatrix}^T$.

The desired state space expression is $\boldsymbol{x}^* = \begin{bmatrix} x_1^* & x_2^* \end{bmatrix}^T = \begin{bmatrix} i_{\text{in}}^* & u_p^* \end{bmatrix}^T$, where i_{in}^* and u_p^* represent the inductor's desired current and desired output voltage, respectively. The PBC ultimately results in the state variable x reaching the value of x^*. The state vector error is set as $\boldsymbol{e} = x - x^*$.

Usually, the EL model based on the PBC theory could be expressed as:

$$\boldsymbol{A}\frac{\mathrm{d}\boldsymbol{e}}{\mathrm{d}t} + \boldsymbol{R}\boldsymbol{e} = \boldsymbol{U} - \left(\boldsymbol{A}\frac{\mathrm{d}\boldsymbol{x}^*}{\mathrm{d}t} + \boldsymbol{B}\boldsymbol{x} + \boldsymbol{R}\boldsymbol{x}^*\right), \tag{3}$$

where $\dfrac{\mathrm{d}\boldsymbol{e}}{\mathrm{d}t}$ denotes the derivative of the error, $\dfrac{\mathrm{d}\boldsymbol{x}^*}{\mathrm{d}t}$ represents the derivative of x^*, and the error function of the system is:

$$\boldsymbol{H}_{\boldsymbol{e}}(\boldsymbol{x}) = \frac{1}{2}\boldsymbol{e}^T\boldsymbol{A}\,\boldsymbol{e}. \tag{4}$$

In order to let the error energy storage function converge to zero at the greatest possible speed, it is necessary to inject damping into the system. The injected damping can be expressed as R_p.

$$\boldsymbol{R_a e} = \left(\boldsymbol{R}_p + \boldsymbol{R}\right)\boldsymbol{e}, \tag{5}$$

where $\boldsymbol{R}_p = \begin{bmatrix} R_{1p} & 0 \\ 0 & \dfrac{1}{R_{2p}} \end{bmatrix}$, $R_{1p} > 0$, $R_{2p} > 0$.

By substituting $\boldsymbol{e} = x - x^*$ into (2) and adding the damping matrix to both sides of the equation, the error model of the Euler-Lagrange (EL) could be expressed as [28].

$$\boldsymbol{A}\frac{\mathrm{d}\boldsymbol{e}}{\mathrm{d}t} + \boldsymbol{R}\,\boldsymbol{e} + \boldsymbol{R}_p\boldsymbol{e} = \boldsymbol{U} - \left(\boldsymbol{A}\frac{\mathrm{d}\boldsymbol{x}^*}{\mathrm{d}t} + \boldsymbol{B}\,\boldsymbol{x} + \boldsymbol{R}\,\boldsymbol{x}^*\right) + \boldsymbol{R}_p\boldsymbol{e}. \tag{6}$$

Furthermore, the controller of PBC could be denoted as follows:

$$\boldsymbol{U} = \boldsymbol{A}\frac{\mathrm{d}\boldsymbol{x}^*}{\mathrm{d}t} + \boldsymbol{B}\,\boldsymbol{x} + \boldsymbol{R}\,\boldsymbol{x} - \boldsymbol{R}_p\boldsymbol{e}. \tag{7}$$

3.2. Fixed switching frequency MPC-based nonlinear design of the boost converter

If the sampling frequency in (1) is sufficiently high, the Euler discretization method can be used to discretize it, leading to the following:

$$\begin{cases} u_p(m+1) = u_p(k) + \dfrac{T_s}{C}\left[i_L(m)(1-s) - \dfrac{u_p(m)}{R}\right], \\ i_{\mathrm{in}}(m+1) = i_{\mathrm{in}}(m) + \dfrac{T_s}{L}u_{\mathrm{in}} - \dfrac{T_s}{L}u_p(m)(1-s). \end{cases} \tag{8}$$

According to (8), i_{in} and u_p at the moment $m+1$ can be predicted, and m represents the current moment. Meanwhile, the discrete sampling time is T_s.

The objective of MPC is typically to ensure that the converter provides a stable output voltage to the load. The most direct method for controlling the output voltage is to employ the cost function, which is followed by the direct inductor current MPC, and based on the aforementioned cost function. Subsequently, the cost function for MPC is constructed.

$$\begin{cases} J_1 = \displaystyle\sum_{k=1}^{N}\left(i_{\mathrm{in}}^*(m) - i_{\mathrm{in}}(m+1)\right)^2, \\ J_2 = \displaystyle\sum_{k=1}^{N}\left(u_p^*(m) - u_p(m+1)\right)^2. \end{cases} \tag{9}$$

Then, this paper proposes further enhancement by re-modifying the differential equation of i_{in}. It is achieved by ensuring that the input power is tantamount to the output power, which is obtained as:

$$i_{\mathrm{in}} = \frac{u_p i_o}{u_{\mathrm{in}}}, \tag{10}$$

where i_o is the system's output current. Then it is substituted to the (8), while (11) is obtained, in the following form:

$$\begin{cases} u_p(m+1) = u_p(k) + \dfrac{T_s}{C}\left[i_{\mathrm{in}}(m)(1-s) - \dfrac{u_p(m)}{R}\right], \\ i_{\mathrm{in}}(m+1) = i_{\mathrm{in}}(m) + \dfrac{T_s}{L}u_{\mathrm{in}} - \dfrac{T_s}{L}\sqrt{i_{\mathrm{in}}(m)u_{\mathrm{in}}R}(1-s). \end{cases} \tag{11}$$

Substituting the $u_p(m+1)$, $i_{\mathrm{in}}(m+1)$ calculated in (11) into (9) to obtain the cost function for single-step optimization MPC is expressed as:

$$J = \left(i_{\mathrm{in}}(m) - \frac{(1-s)}{L}\sqrt{i_{\mathrm{in}}(m)u_{\mathrm{in}}RT_s} + \frac{1}{L}u_{\mathrm{in}}T_s - i_{\mathrm{in}}^*\right)^2 + \left(u_p(m) + \frac{(1-s)}{C}i_{\mathrm{in}}(m)T_s - \frac{1}{RC}u_p(m)T_s - u_p^*\right)^2. \tag{12}$$

In order to get the control signal, this paper establishes a direct correlation between the duty cycle and MPC.

$$\frac{\partial J}{\partial s} = \frac{\partial\left[\left(i_{\mathrm{in}}(m+1) - i_{\mathrm{in}}^*\right)^2 + \left(u_p(m+1) - u_p^*\right)^2\right]}{\partial s} = 0. \tag{13}$$

By the tenets of (13), (14) is obtained:

$$D = \frac{\left(i_{\mathrm{in}}(m) - \dfrac{1}{L}\sqrt{i_{\mathrm{in}}(m)u_{\mathrm{in}}RT_s} + \dfrac{1}{L}u_{\mathrm{in}}T_s - i_{\mathrm{in}}^*\right)\dfrac{1}{L}\sqrt{i_{\mathrm{in}}(m)u_{\mathrm{in}}RT_s}}{-\dfrac{1}{C^2}i_{\mathrm{in}}(m)^2T_s^2 - \dfrac{1}{L^2}i_{\mathrm{in}}(m)u_{\mathrm{in}}RT_s^2} - \frac{\left(u_p(m) + \dfrac{1}{C}i_{\mathrm{in}}(m)T_s - \dfrac{1}{RC}u_p(m)T_s - u_p^*\right)\dfrac{1}{C}i_{\mathrm{in}}(m)T}{-\dfrac{1}{C^2}i_{\mathrm{in}}^2(m)T_s^2 - \dfrac{1}{L^2}i_{\mathrm{in}}(m)u_{\mathrm{in}}RT_s^2}. \tag{14}$$

In this scenario, the cost function will attain its minimal value upon the adoption of the optimally derived variable D.

3.3. The proposed FSF-PBMPC nonlinear design for the boost converter

To further accelerate the system's response speed and to reduce the computational complexity of MPC, this paper aims to combine PBC and the fixed switching frequency MPC, named fixed switching frequency MPC based on passivity-based control. The model based on the proposed control strategy could be expanded as:

$$\begin{cases} u_{\mathrm{in}} = L\dfrac{\mathrm{d}i_{\mathrm{in}}^*}{\mathrm{d}t} + (1-s)u_p - R_{1p}\left(i_{\mathrm{in}} - i_{\mathrm{in}}^*\right), \\ 0 = C\dfrac{\mathrm{d}u_p^*}{\mathrm{d}t} - (s-1)i_{\mathrm{in}} + \dfrac{1}{R}u_p^* - \dfrac{1}{R_{2p}}\left(u_p - u_p^*\right). \end{cases} \tag{15}$$

(15) represents the PBC equation. Furthermore, i_{in}^* and u_p^* are the reference values of i_{in} and u_p, respectively. Thus, $\dfrac{\mathrm{d}i_{\mathrm{in}}^*}{\mathrm{d}t} = 0$, $\dfrac{\mathrm{d}u_p^*}{\mathrm{d}t} = 0$. Therefore, the electrical subsystem can be

described as:

$$\begin{cases} i_{\text{in}}(m) = \dfrac{1}{R_{1p}}\left[(1-s)u_p(m) - u_{\text{in}}(m)\right] + i_{\text{in}}^*(m), \\ u_p(m) = R_{2p}\left[(s-1)i_{\text{in}}(m) + \dfrac{1}{R}u_p^*(m)\right] + u_p^*(m). \end{cases} \tag{16}$$

From this, it can be concluded that:

$$u_p(m) = \frac{u_{\text{in}} i_{\text{in}}^* R}{u_p^*} + \frac{R_{1p} i_{\text{in}}^* R\left(i_{\text{in}}^* - i_{\text{in}}\right)}{u_p^*}. \tag{17}$$

Substituting (17) into (14), the final control expression is:

$$D = \frac{\left(i_{\text{in}}(m) - \dfrac{1}{L}\sqrt{i_{\text{in}}(m)u_{\text{in}}RT_s} + \dfrac{1}{L}u_{\text{in}}T_s - i_{\text{in}}^*\right)\dfrac{1}{L}\sqrt{i_{\text{in}}(m)u_{\text{in}}RT_s}}{-\dfrac{1}{C^2}i_{\text{in}}(m)^2T_s^2 - \dfrac{1}{L^2}i_{\text{in}}(m)u_{\text{in}}RT_s^2} - \frac{\left(u_p(m) + \dfrac{1}{C}i_{\text{in}}(m)T_s - \dfrac{1}{RC}u_p(m)T_s - u_p^*\right)\dfrac{1}{C}i_{\text{in}}(m)T_s}{-\dfrac{1}{C^2}i_{\text{in}}^2(m)T_s^2 - \dfrac{1}{L^2}i_{\text{in}}(m)u_{\text{in}}RT_s^2}. \tag{18}$$

Figure 3 illustrates the control block of the proposed control strategy for the boost converter.

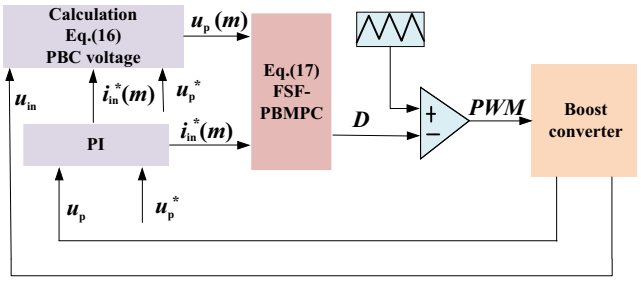

Fig. 3. Control block of the proposed control strategy

3.4. Stability analysis of the proposed method

Since it is difficult to obtain the analytical form of the control loop transfer function for MPC, it leads to the difficulty of the traditional stability analysis methods. In light of the fact that the Lyapunov function does not necessitate the availability of a transfer function, this paper employs it as a foundation for the proof of stability of the proposed control method.

The positive Lyapunov function is denoted as:

$$C = 0.5\left\|i_{\text{in}}^* - i_{\text{in}}(m)\right\|_2^2. \tag{19}$$

As shown in (19), this function is the Euclidean distance between the desired inductor current and the actual current. In this context, the Lyapunov function is represented by the symbol C.

(19) is derived as follows:

$$\dot{C} = -\frac{\mathrm{d}i_{\text{in}}(k)^T}{\mathrm{d}t}\cdot\left(i_{\text{in}}^* - i_{\text{in}}(m)\right). \tag{20}$$

With the model of the boost converter, (20) can be modified as:

$$\dot{C} = -\frac{u_{\text{in}} - (1-s)u_p}{L}\cdot\left(i_{\text{in}}^* - i_{\text{in}}(m)\right). \tag{21}$$

Substituting (17) into (21), the following result is obtained:

$$\dot{C} = -\frac{u_{\text{in}} - (1-s)\dfrac{u_{\text{in}}i_{\text{in}}^*R}{u_p^*} + \dfrac{R_{1p}\left(i_{\text{in}}^* - i_{\text{in}}(m)\right)}{u_p^*}}{L}\cdot\left(i_{\text{in}}^* - i_{\text{in}}(m)\right) - \frac{\mathrm{d}i_{\text{in}}^*(m)^T}{\mathrm{d}t}\left(i_{\text{in}}^* - i_{\text{in}}(m)\right), \tag{22}$$

where $\dfrac{\mathrm{d}i_{\text{in}}^*(m)^T}{\mathrm{d}t} = 0$. When $s = 0$, (22) is a negative definite, indicating that the system is stable. When $s = 1$, (22) is shown as:

$$\dot{C} = -\frac{u_{\text{in}}u_p^* - R_{1p}\left(i_{\text{in}}^* - i_{\text{in}}(m)\right)}{u_p^*L}\cdot\left(i_{\text{in}}^* - i_{\text{in}}(m)\right). \tag{23}$$

Substituting (16) into (23), (24) is obtained:

$$\dot{C} = -\frac{u_{\text{in}}u_p^* - \dfrac{u_{\text{in}}^2}{R_{1p}}}{u_p^*L}. \tag{24}$$

Thus, it is established that the value is in fact negative, which consequently ensures the stability of the system.

To ensure that the system is stable, the injection damping R_{1p} is selected as 5 Ω.

3.5. Selection of passive controller parameters

The passive controller injection damping R_{1P} variable is proportional to the stored energy of the inductor, whereas the R_{2P} variable depends on the stored energy of the capacitor. In order to ascertain the injection damping values, the inductor series resistance R_1 and the capacitor series resistance R_2 are employed in the following equivalent circuit state-space equations.

The state space equation of the equivalent circuit is shown as:

$$\dot{\boldsymbol{x}} = \begin{bmatrix} -\dfrac{R_1}{L} & -\dfrac{1-D}{L} \\ \dfrac{1-D}{C} & -\dfrac{1}{CR_2} - \dfrac{1}{CR} \end{bmatrix}\boldsymbol{x} + \begin{bmatrix} \dfrac{1}{L} \\ 0 \end{bmatrix}u_{\text{in}}. \tag{25}$$

At this point the characteristic equation of (25) is:

$$s^2 + \left(\frac{R_1}{L} + \frac{1}{CR_2} + \frac{1}{CR}\right)s + \frac{(1-D)^2}{CL} + \frac{R_1}{CL}\left(\frac{1}{R_2} + \frac{1}{R}\right) = 0. \tag{26}$$

In order to relate R_1 and R_2 in the equivalent circuit to the damping injections R_{1p} andR_{2p}, (4) is simplified. It follows that:

$$\boldsymbol{A}\dot{\boldsymbol{e}} = -\boldsymbol{R}_p\boldsymbol{e}. \tag{27}$$

Simplifying through it gives the following:

$$\dot{\boldsymbol{x}} = -\begin{bmatrix} \dfrac{R_{1p}}{L} & 0 \\ 0 & \dfrac{1}{CR_{2p}} \end{bmatrix} \begin{bmatrix} x_1 - x_1^* \\ x_2 - x_2^* \end{bmatrix}. \tag{28}$$

By associating (25) with (28), (29) can be obtained:

$$\begin{cases} R_1 = \dfrac{u_{\text{in}} + R_{1p} i_{\text{in}} - R_{1p} i_{\text{in}}^* - (1-D)u_p}{i_{\text{in}}}, \\ \dfrac{1}{R_2} = \dfrac{R}{CR_{1p}}\left(1 - \dfrac{u_p^*}{u_p}\right) + \dfrac{R}{Cu_p}(1-D)i_{\text{in}} - \dfrac{1}{C}. \end{cases} \tag{29}$$

At steady state $u_{\text{in}} - i_{\text{in}} R_{1p} = (1-D)u_p$, $i_{\text{in}} = i_{\text{in}}^*$, we can get:

$$\begin{cases} R_1 = R_{1p}, \\ \dfrac{1}{R_2} = 0. \end{cases} \tag{30}$$

Substituting (30) into (26) yields the equation characterizing the virtual equivalent circuit:

$$s^2 + \left(\frac{R_{1p}}{L} + \frac{1}{CR}\right)s + \frac{(1-D)^2}{CL} + \frac{R_{1p}}{CLR} = 0. \tag{31}$$

At this point, the damping ratios ξ and R_{1p} of the system are, respectively:

$$\begin{cases} \xi = \dfrac{\dfrac{R_{1p}}{L} + \dfrac{1}{CR}}{2\sqrt{\dfrac{(1-D)}{CL} + \dfrac{R_{1p}}{CLR}}}, \\ R_{1p} = \dfrac{(2\xi^2 - 1)L}{CR} + \sqrt{\left(\dfrac{2\xi^2 L - L}{CR}\right)^2 + \dfrac{4(1-D)\xi^2 L}{C}}. \end{cases} \tag{32}$$

The output voltage response of the closed-loop system under the action of the unit step signal is shown in Fig. 4 for damping ratios of 0.1, 0.5, 1, 1.5 and 2, respectively. It can be observed that when the damping ratio falls between 0 and 1, indicating an under-damped state, the transient response of the system exhibits a sinusoidal oscillation curve with an amplitude that decays exponentially. In the case of $\zeta = 1$ or $\zeta > 1$, the system is in the critical damping or over-damping state, and the transient response of the system presents a monotonically rising exponential curve, with no oscillation occurring. This indicates that the passive system is more stable. At this juncture, the value of R_{1p} should satisfy the following:

$$R_{1p} \geq \frac{L}{CR} + \sqrt{\frac{L^2}{C^2R^2} + \frac{4(1-D)L}{C}}. \tag{33}$$

Combining the L and C parameters, $R_{1p} = 5\ \Omega$ is chosen in this paper.

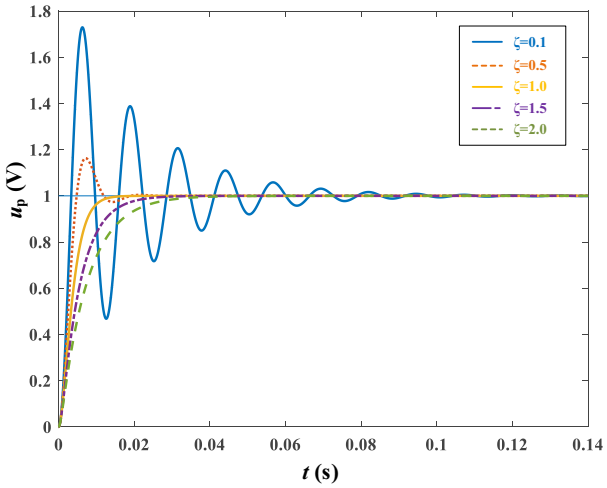

Fig. 4. Unit step response curve of the system

4. SIMULATION RESULTS

This paper employs the boost converter as a case study for the verification of simulation results. Firstly, the fixed-switching frequency MPC is contrasted and analyzed with the non-fixed-switching frequency MPC. It is demonstrated that the interference immunity of the MPC is enhanced after fixing the switching frequency. Secondly, the simulation results are conducted for five cases, including inductance and capacitance change, sudden change of desired voltage, load, and input voltage. The simulation results demonstrate the efficacy of the proposed methodology. The parameters which are employed in the simulation are presented in Table 1. The calculation process of the proposed FSF-PBMPC is shown as Table 2.

Table 1
System simulation parameters

Parameter name	Symbol	Value	Unit
DC input voltage	u_{in}	50	V
Desired DC output voltage	u_p^*	100	V
Inductors	L	1.5	mH
Capacitors	C	1500	uF
Injection damping	R_{1p}	5	Ω
Switching frequency	f	20	kHz
Load resistance	R	50	Ω
Proportionality	K_P	0.8	
Integral adjustment	K_i	160	
Sampling time	T_s	60	us

According to the parameter values given in Table 1, we compare and analyze the proposed control method with fixed-switching frequency MPC in the boost converter based on simulation results under varying input voltage, desired voltage and load disturbance. Table 2 illustrates the calculation process of the implementation of the algorithm.

Table 2
System simulation parameters

Algorithm 1. FSF-PBMPC Algorithm
function FSF-PBMPC
1. Measure u_{in}, i_{in}
2. Collecting values of i^*_{in}
3. Setting the value of u^*_p
2. Calculate equation (17)
3. Calculate equation (18)
end
end function
Update D

4.1. Comparative analysis of non-fixed-switching frequency MPC and fixed-switching frequency MPC

Figure 5 depicts the simulation results of the conventional MPC without fixed switching frequency. The variability of the controller can be observed. The controller's effect cannot be realized accurately, as indicated by the output voltage and output current ripple plots, as it will result in a non-uniform i_{in} and u_p.

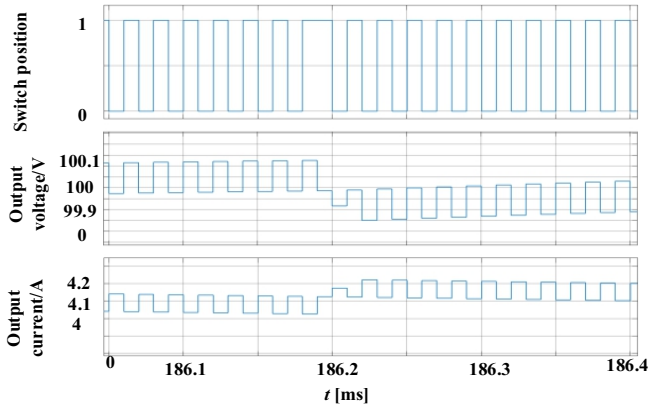

Fig. 5. Non-fixed-switching frequency MPC

Figure 6 displays the simulation results of the fixed switching frequency MPC, demonstrating the achieved outcomes of the fixed switching frequency MPC. The controller's effectiveness is accurately demonstrated by the output voltage's ripple diagrams and output current's ripple diagrams, resulting in a uniform inductor current and output voltage.

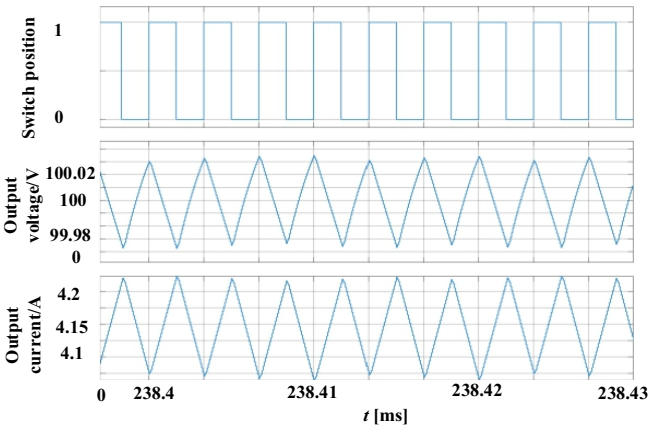

Fig. 6. Fixed-switching frequency MPC

The results demonstrate that the stability of the system of the fixed-switching frequency MPC is enhanced. The controller's effectiveness is accurately demonstrated by the output voltage's ripple diagrams and output current's ripple diagrams.

4.2. Simulation of inductance and capacitance change

The simulated waveform of the u_p and i_o of the boost converter when the inductance and capacitance are performed is shown in Fig. 7 and Fig. 8.

Figure 7 shows the simulation results for the output voltage and output current as the inductance parameter is changed. To evaluate the effectiveness of the proposed control method, a graph of the control for FSF-PBMPC was generated where the inductance parameter of the circuit was increased from its original value of 1 mH to 2 mH. After increasing the inductance, it was observed that the voltage and current fluctuations were minimal, as was the ripple fluctuation amplitude. Thus, the effect of the inductance parameter on the circuit was found to be insignificant, thus verifying the robustness of the method with respect to this parameter.

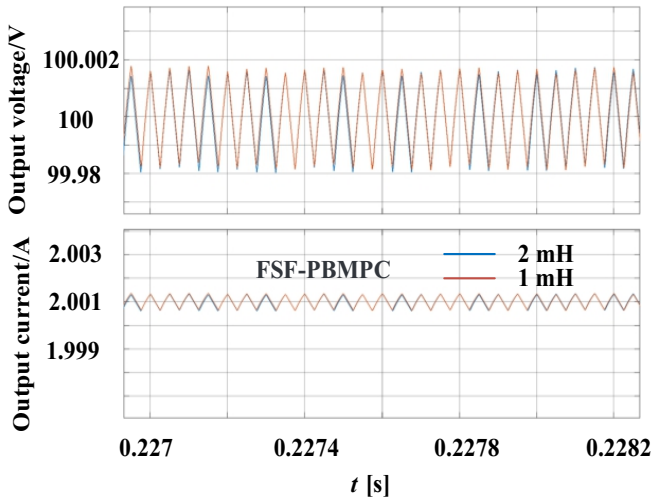

Fig. 7. FSF-PBMPC inductance increase comparison – simulation results

Figure 8 illustrates the simulation result graph of the output voltage and output current after increasing the capacitance parameter. The capacitance parameter of the circuit is increased from 1500 µF to 2000 µF. Furthermore, an increase in capacitance resulted in a reduction in voltage and current fluctuations, as well as a decrease in ripple fluctuation amplitude. The impact on the circuit was also found to be minimal. Consequently, the robustness of this method was verified in terms of the capacitance parameter. The impact on the circuit is minimal, thus verifying the robustness of the method in terms of capacitance parameters.

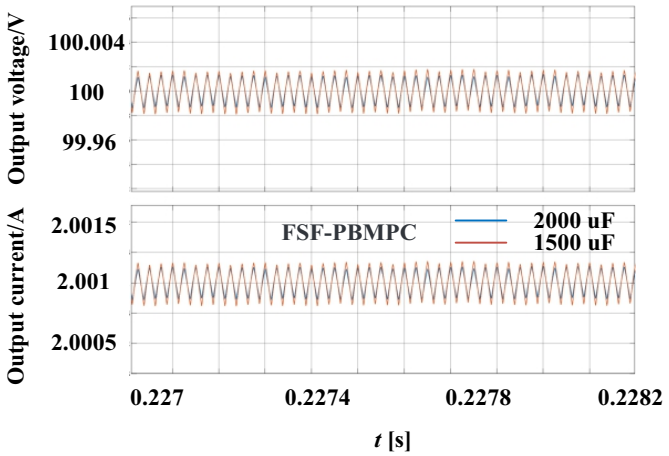

Fig. 8. FSF-PBMPC capacitance increase comparison – simulation results

4.3. Simulation of desired voltage change

The simulated waveform of the u_p and i_o of the boost converter when the desired voltage changes is performed is shown in Fig. 9. We compare the stabilization and response speed of these two control strategies under varying desired voltage conditions.

Figure 9 illustrates the waveforms of u_p and i_o when the desired output voltage is altered. The initial voltage is set to 50 V, the initial u_p^* is set to 70 V, and then u_p^* is set to 100 V at 0.3 s. The addition of PBC accelerates the system's dynamic response, and the overshoot of the system is reduced.

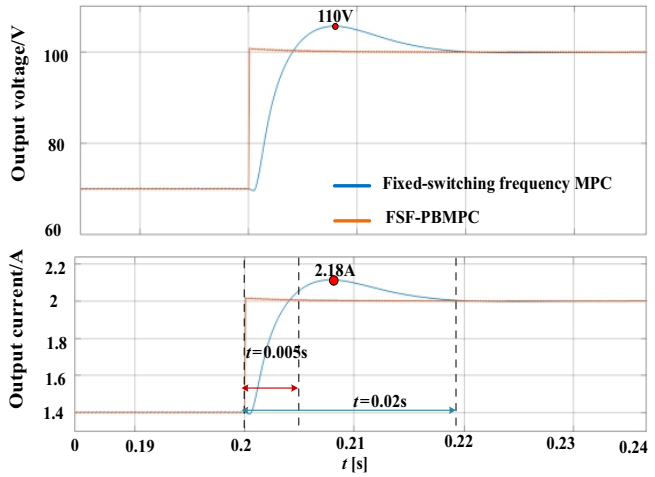

Fig. 9. Comparison of desired voltage change simulation of fixed-frequency MPC and proposed control

4.4. Simulation of load disturbance change

In Fig. 10, the waveforms of the u_p and i_o of the system when the load is varied are presented. The initial voltage is 50 V, and u_p^* is 100 V. The initial load is set to 50 Ω, and a 50 Ω resistor is connected in parallel at both ends of the load at 0.3 s. The total resistance is 25 Ω. As illustrated in the graph, the dynamic response of the proposed control is more rapid, and there is no overshooting in the process.

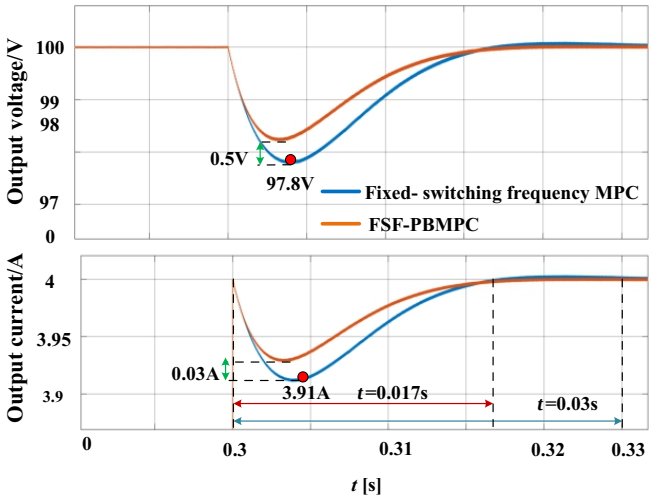

Fig. 10. Comparison of load disturbance change simulation of fixed-frequency MPC and proposed control

4.5. Simulation of input voltage change

Figure 11 shows the waveforms of u_p and i_o when u_{in} is varied. To begin with, u_{in} is 50 V and u_p^* is 100 V. At 0.3 s, u_{in} is varied from 50 V to 60 V. As illustrated in the figure, the overshoot is reduced and the dynamic response is accelerated for the proposed control.

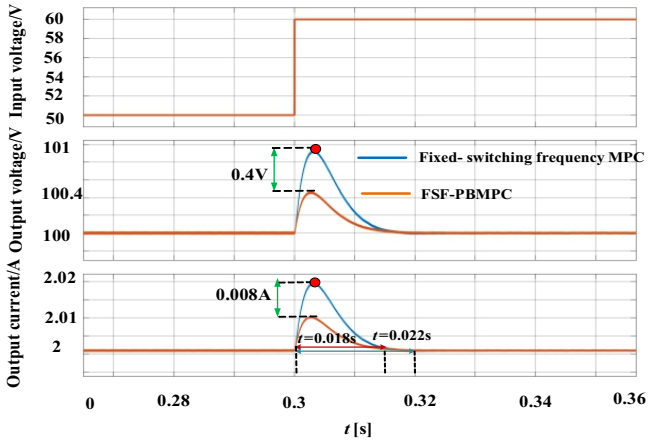

Fig. 11. Comparison of input voltage change simulation of fixed-switching frequency MPC and proposed control

The simulation verification is conducted under five scenarios: inductance and capacitance change, sudden changes in the desired voltage, load and the input voltage. The results indicate that the stability of the fixed switching frequency MPC is enhanced by the addition of PBC, while the dynamic response speed of the system is accelerated.

5. CONCLUSIONS

In this paper, a nonlinear control strategy named FSF-PBMPC is proposed, which is based on the FCS-MPC method and passive-based control theory. Firstly, the switching signals generated by the traditional model prediction are converted to the optimal

duty cycle, thereby generating a fixed switching frequency. Secondly, passivity-based control is incorporated into the MPC framework in order to enhance the stability of the system and accelerate the system's response speed. The efficacy of the proposed method is validated through simulation based on MATLAB, leading to the following conclusions.

1. The system's stability is improved under the proposed FSF-PBMPC control strategy with a fixed switching frequency. It is observed that the uniform inductor current and output voltage control effect is realized.
2. Compared with the fixed-frequency MPC, the proposed FSF-PBMPC method enhances the system's anti-interference capability and improves the response speed by incorporating passive-based control. Furthermore, the proposed control strategy has faster dynamic response speed and no overshoot when the simulation conditions are varied.
3. The proposed control strategy is capable of adapting to changes in operating conditions.

ACKNOWLEDGEMENTS

Project supported by the Headquarters Technology Projects of State Grid Corporation of China (5200-202456095A-1-1-ZN) and the National Natural Science Foundation of China (52237008).

REFERENCES

[1] T. Dragičević, X. Lu, J.C. Vasquez, and J.M. Guerrero, "DC Microgrids-Part I: A Review of Control Strategies and Stabilization Techniques," *IEEE Trans. Power Electron.*, vol. 31, no. 7, pp. 4876–489, 2016, doi: 10.1109/TPEL.2015.2478859.

[2] Z. Karami, Q. Shafiee, S. Sahoo, M. Yaribeygi, H. Bevrani, and T. Dragicevic, "Hybrid Model Predictive Control of DC–DC Boost Converters With Constant Power Load," *IEEE Trans. Energy Convers.*, vol. 36, no. 2, pp. 1347–1356, 2021, doi: 10.1109/TEC.2020.3047754.

[3] A. Reatti, F. Corti, A. Tesi, A. Torlai, and M.K. Kazimierczuk, "Nonlinear Exact Analysis and Solution of Power Stage of DC-DC PWM Boost Converter," in *2019 IEEE Int. Symp. Circuits and Syst. (ISCAS)*, 2019, pp. 1–5, doi: 10.1109/ISCAS.2019.8702549.

[4] Z. Junzi, L. Ye, Y. Yuanyuan, H. Fuhua, and Z. Xiaoqi, "A Novel Adaptive Control Strategy for Transient Performance Improvement of DC/DC Converter in Distributed Power Generation Systems," in *2022 IEEE/IAS Ind. and Commercial Power Syst. Asia (I&CPS Asia)*, 2022, pp. 570–576, doi: 10.1109/ICPSAsia55496.2022.9949908.

[5] P. Karamanakos, T. Geyer, and S. Manias, "Direct Voltage Control of DC–DC Boost Converters Using Enumeration-Based Model Predictive Control," *IEEE Trans. Power Electron.*, vol. 29, no. 2, pp. 968–978, 2014, doi: 10.1109/TPEL.2013.2256370.

[6] L. Karunaratne, N.R. Chaudhuri, A. Yogarathnam, and M. Yue, "Nonlinear Backstepping Control of Grid-Forming Converters in Presence of Grid-Following Converters and Synchronous Generators," *IEEE Trans. Power Syst.*, vol. 39, no. 1, pp. 1948–1964, 2024, doi: 10.1109/TPWRS.2023.3272528.

[7] J.H. Urrea-Quintero, N. Muñoz-Galeano, and D.A. Cuervo-Sanchez, "A procedure for power electronic converters design with controllability verification based on the nonlinear dynamical model," in *2017 IEEE Workshop Power Electron. and Power Qual. Appl. (PEPQA)*, 2019, pp. 1–6, doi: 10.18178/ijeee.5.3.207-212.

[8] F. Wang, G. Lin, and Y. He, "Passivity-Based Model Predictive Control of Three-Level Inverter-Fed Induction Motor," *IEEE Trans. Power Electron.*, vol. 36, no. 2, pp. 1984–1993, 2021, doi: 10.1109/TPEL.2020.3008915.

[9] L. Qiu, "Passivity-Based Cascade-Free Finite-Set Model Predictive Control for Nested Neutral Point-Clamped Converters," *IEEE Access*, vol. 8, pp. 200209–200218, 2020, doi: 10.1109/ACCESS.2020.3033272.

[10] Z. Yu, J. Zeng, J. Liu, and F. Luo, "Terminal sliding mode control for dual active bridge dc-dc converter with structure of voltage and current double closed loop," in *2018 Australian & New Zealand Control Conf. (ANZCC)*, 2018, pp. 11–15, doi: 10.1109/ANZCC.2018.8606608.

[11] H. Sira-Ramirez, G. Escobar, and R. Ortega, "On passivity-based sliding mode control of switched DC-to-DC power converters," in *Proc. of 35th IEEE Conf. Decision and Control*, 1996, pp. 2525–2526, doi: 10.1109/CDC.1996.573474.

[12] F. Tlili and F. Bacha, "Fuzzy Logic Direct Power Control of a Bidirectional Three-Phase ACIDC Converter," in *2020 20th Int. Conf. Sciences and Techn. Autom. Control and Comput. Eng. (STA)*, 2020, pp. 201–206, doi: 10.1109/STA50679.2020.9329316.

[13] A. Ghosh and S. Banerjee, "A Comparison between Classical and Advanced Controllers for a Boost Converter," in *2018 IEEE Int. Conf. Power Electron., Drives and Energy Syst. (PEDES)*, 2018, pp. 1–6, doi: 10.1109/PEDES.2018.8707911.

[14] J. Liu, W. Ming, and F. Gao, "A new control strategy for improving performance of boost DC/DC converter based on input-output feedback linearization," in *2010 8th World Congr. Intel. Control and Autom.*, 2010, pp. 2439–2444, doi: 10.1109/WCICA.2010.5554675.

[15] B. Taheri and M. Sedaghat, "A new general controller for DC-DC converters based on SMC methods," in *2018 6th Int. Istanbul Smart Grids and Cities Congr. and Fair (ICSG)*, 2018, pp. 49–53, doi: 10.1109/SGCF.2018.8408940.

[16] N. Vafamand, S. Yousefizadeh, M.H. Khooban, J.D. Bendtsen, and T. Dragičević, "Adaptive TS Fuzzy-Based MPC for DC Microgrids With Dynamic CPLs: Nonlinear Power Observer Approach," *IEEE Syst. J.*, vol. 13, no. 3, pp. 3203–3210, 2019, doi: 10.1109/JSYST.2018.2880135.

[17] J. Zeng, Z. Zhang, and W. Qiao, "An Interconnection and Damping Assignment Passivity-Based Controller for a DC–DC Boost Converter With a Constant Power Load," *IEEE Trans. Ind. Appl.*, vol. 50, no. 4, pp. 2314–2322, 2014, doi: 10.1109/TIA.2013.2290872.

[18] L. Gupta, S. Bhandari, and Deepika, "Modelling of Passivity based Controller for Buck Boost Converter," in *2022 2nd Int. Conf. Next Gener. Intell. Syst. (ICNGIS)*, 2022, pp. 1–6, doi: 10.1109/ICNGIS54955.2022.10079798.

[19] W. Ao and J. Chen, "Model Predictive Control of Four-Switch Buck-Boost Converter for Pulse Power Loads," in *2021 IEEE Int. Conf. Predictive Control Elect. Drives and Power Electron. (PRECEDE)*, 2021, pp. 904–908, doi: 10.1109/PRECEDE51386.2021.9680981.

[20] S. Ni, Z. Zheng, L. Peng, and Y. Li, "A Hybrid PI-FOC and CCS-MPC Method for Multiple Harmonic Current Suppression

in Multiphase Machines," in *2023 IEEE Int. Conf. Predictive Control Elect. Drives and Power Electron. (PRECEDE)*, 2023, pp. 1–7, doi: 10.1109/PRECEDE57319.2023.10174487.

[21] A. Choubey, P.K. Padhy and S.K. Jain, "Model Predictive Control for DC-DC Boost converter," in *2021 IEEE Conf. Energy Convers. (CENCON)*, 2021, pp. 58–63, doi: 10.1109/CENCON51869.2021.9627268.

[22] Y. Song, "Research on Control Strategy of Three-level PV Grid-Connected Inverter Based on FCS-MPC," in *2023 4th Int. Conf. Adv. Elect. and Energy Syst. (AEES)*, 2023, pp. 39–44, doi: 10.1109/AEES59800.2023.10468919.

[23] Y. Li, S. Sahoo, T. Dragičević, Y. Zhang, and F. Blaabjerg, "Stability-Oriented Design of Model Predictive Control for DC/DC Boost Converter," *IEEE Trans. Ind. Electron.*, vol. 71, no. 1, pp. 922–932, 2024, doi: 10.1109/TIE.2023.3247785.

[24] P. Karamanakos and T. Geyer, "Guidelines for the Design of Finite Control Set Model Predictive Controllers," *IEEE Trans. Power Electron.*, vol. 35, no. 7, pp. 7434–7450, 2020, doi: 10.1109/TPEL.2019.2954357.

[25] M.S. Mousavi, S.A. Davari, V. Nekoukar, C. Garcia, and J. Rodriguez, "A Robust Torque and Flux Prediction Model by a Modified Disturbance Rejection Method for Finite-Set Model-Predictive Control of Induction Motor," *IEEE Trans. on Power Electron.*, vol. 36, no. 8, pp. 9322–9333, 2021, doi: 10.1109/TPEL.2021.3054242.

[26] X. Zhang, H. Zhang, and K. Yan, "Hybrid Four-segment-mode Model Predictive Control for Open-winding PMSM Drives," *IEEE Trans. Transp. Electrific.*, vol. 10, no. 2, pp. 4322–4333, 2024, doi: 10.1109/TTE.2023.3308570.

[27] N. Guler, S. Biricik, S. Bayhan, and H. Komurcugil, "Model Predictive Control of DC–DC SEPIC Converters With Autotuning Weighting Factor," *IEEE Trans. Indus. Electron.*, vol. 68, no. 10, pp. 9433–9443, Oct. 2021, doi: 10.1109/TIE.2020.3026301.

[28] Y. Li, T. Dragičević, S. Sahoo, Y. Zhang, and F. Blaabjerg, "An Improved Model Predictive Control for DC-DC Boost Converter," in *2022 IEEE 13th Int. Symp. Power Electron. Distrib. Gener. Syst. (PEDG)*, 2022, pp. 1–6, doi: 10.1109/PEDG54999.2022.9923104.